A new formulation for dendritic crystal growth in two dimensions

E.A. Coutsias* and H. Segur
* U. of New Mexico, Albuquerque 87131
U. of Colorado, Boulder 80309-0526

September 16, 2003

Abstract

The objective of this paper is to study the growth of dendritic crystals in two spatial dimensions plus time. The paper makes three contributions. (i) We propose a new dynamic criterion to test physical mechanisms that might produce the velocity selection that is observed experimentally. We have not yet determined how the results of this criterion compare with those obtained by other criteria, such as microscopic solvability. (ii) The (known) equations of motion are restated in terms of orthogonal parabolic coordinates, a natural coordinate system in which to study perturbations of a parabolic (Ivantsov) interface. Among its other advantages, this formulation permits a larger class of behaviours far from the tip of the crystal than is allowed in the usual representation. (iii) On an initially parabolic interface, the analogue of the Mullins-Sekerka instability is more delicate than previously had been assumed. In particular, we find numerically that the range of unstable "wavenumbers" is bounded away from zero; i.e., sufficiently low wavenumbers are stable. Moreover, our preliminary calculations show parabolae, characterised by Peclet numbers of order 1, for which the linear instability is completely suppressed by enough surface tension. Such suppression is impossible on a flat interface.

1 Introduction

Of all of the physical problems discussed at this workshop, perhaps none has been more influential in distilling the fundamental concepts of the subject of Asymptotics Beyond All Orders than the problem of growing dendritic crystals. Within these Proceedings, all of the papers on the geometric model indirectly address the problem of dendritic crystals. Moreover, the papers by Gollub [6], Kessler [9], and Levine [15] (also in these Proceedings) discuss aspects of the hypothesis of "microscopic solvability", which asserts that the tip of a dendritic crystal grows with a constant velocity determined by a transcendentally small quantity related to the surface tension.

A complete statement of the problem can be found in the papers just cited. Briefly, experiments show that when a dendritic crystal grows into a slightly supercooled melt, the shape of the moving interface between the (liquid) melt and the (solid) crystal is inherently unsteady and complicated, but also that the tip of the crystal moves with a nearly constant velocity, and with a nearly constant shape. (For a demonstration, see Figure 1 of Gollub, in these Proceedings, or [4], [5].) The steady-state model of Ivantsov [8] predicts that the temperature in the melt far from the crystal ("the undercooling") determines a dimensionless product of the tip radius and the tip velocity ("the Peclet number"), but not their separate values. Thus Ivantsov's model is too simple, in the sense that some physical effect omitted from Ivantsov's model selects a particular tip speed. The question is:
Which physical effects should be added to Ivantsov's model, to create a more complicated model in which both the tip speed and the tip radius are selected by the undercooling?
Candidates include: surface tension along the interface, with or without crystalline anisotropy, interfacial kinetics, and others.

In the presence of surface tension (or any of the other candidates mentioned above), Ivantsov's parabolic crystals no longer solve the equations of (steadily growing) motion. The hypothesis of microscopic solvability asserts that the physical mechanism that selects the tip velocity is the one for which the equations of motion admit a steadily growing, nearly parabolic interface, and the (nearly) parabolic tip that is observed is the one that grows steadily. If the equations admit more than one steadily growing interface shape, then the observed shape is the one that is dynamically stable. This hypothesis has led to the conclusion that surface tension with crystalline anisotropy provides the selection mechanism observed experimentally (cf. Barbieri et al. [1], BenAmar and Pomeau [2], Caroli et al. [3], Kessler and Levine [11], Meiron [16], Saito et al. [20]). Within these proceedings, see Levine [15] for a more complete statement of this approach, and see Gollub [6] for a comparison of the predictions of this model with experimental observations.

While this approach has been succesful in several respects, we feel that it suffers from two logical weaknesses.

1) The question of whether a steadily growing solution exists or not turns out to depend fundamentally, and very delicately, on boundary conditions imposed on the shape of the interface far from the tip of the crystal. However, real crystals are inherently unsteady (and very messy) far from their tips, so it is hard to imagine that steady boundary conditions imposed there ought to play an important role in the selection of the tip velocity.

2) The notions of a steadily growing solution, and of the dynamic stability of such a solution, both are relevant in the limit $t \to \infty$. However, real crystals apparently select their velocities rather quickly (e.g., after encountering an impurity), so an appropriate theory also ought to provide a mechanism to select a velocity on a fairly short time scale.

The primary objective of the research reported here is to formulate an alternative model to microscopic solvability, one that is free of the logical difficulties mentioned above. Our alternative hypothesis is stated in Section 2. The first step in implementing the hypothesis is to recast the equations of motion in parabolic coordinates; this reformulation is given in Section 3. In Section 4 we linearize these equations about an Ivantsov parabola, to obtain approximate equations governing the growth of an interface on a short time scale. (Our hypothesis is that the tip velocity is selected on this short time scale.) The homogeneous solutions of this linearized problem provide the analogue, on a parabolic interface, of the celebrated instability found by Mullins and Sekerka [19] on a flat interface. This instability is analyzed and discussed in Section 5. Our analysis indicates that the parabolic geometry changes the instability in fundamental ways, which apparently had not been noticed before.

2 A dynamic criterion for the selection of dendritic crystals

Our criterion is based on three assumptions:
(i) A growing dendritic crystal is inherently unsteady, except in the immediate neighborhood of the tip.
(ii) Selection of the tip velocity is done on a relatively short time scale.
(iii) The tip velocity is selected by some physical effect that is a small perturbation to the balance inherent in Ivantsov's model (in which latent heat, created at the interface, is carried away by diffusion).

In this paper, we demonstrate our proposed criterion by deriving the equations to determine whether surface tension, with or without crystalline anisotropy, can select a tip velocity in two spatial dimensions. We emphasize that the approach is not restricted to these physical effects.

Let us conduct a thought experiment, in which a crystal is growing steadily into an undercooled melt in two dimensions. For $t < 0$, there is no surface tension, and the undercooling would permit any one of an entire family of Ivantsov's parabolic crystals to grow. Pick one parabola from the family (i.e., select a velocity).

For $t \geq 0$, we turn on a small amount of surface tension. Now the parabolic interface is no longer an equilibrium solution, and the interface will deform. For short times, the size of the deformation will be proportional to the surface tension, and one can linearize the equations about the parabolic shape. We assume that the tip velocity is selected on this short time scale, so these linearized equations contain the selection mechanism, if one exists.

The time-dependent deformation of the interface away from its initially parabolic shape is essentially the Mullins-Sekerka [19] instability, but on a parabolic front. As one might expect, different wavelengths have different growth-rates. We apply the following selection criterion:
Given the initially parabolic shape of the interface, with its own tip velocity, does the resulting (Mullins-Sekerka) instability appear in the neighborhood of the tip? If so, then this particular parabola is not selected by surface tension. We say that a particular parabola is selected by surface tension only if the observed instability leaves quiescent a neighborhood of the tip. If no parabola is selected in this way, then we conclude that surface tension does not provide a selection mechanism.

The equations required to implement this criterion, derived in Sections 3 and 4, are simi-

lar to those previously obtained by Langer and Müller-Krumbhaar [13], with two significant differences.
(i) They were interested in questions of stability (as $t \to \infty$) of the parabolic front, which led them into delicate questions about boundary conditions far from the tip, and which eventually spawned the hypothesis of microscopic solvability. In the model proposed here, stability is irrelevant because the tip velocity is selected on a short time scale, and delicate questions about boundary conditions never arise.
(ii) Our linearized equations are obtained by expanding in the (small) surface tension parameter. However, this parameter multiplies the curvature (i.e., the highest derivative) in the Gibbs-Thomson condition, so the expansion becomes disordered for perturbations of sufficiently short wavelength. To overcome this difficulty, we include in our leading-order perturbation equations a higher-derivative term proportional to the surface tension. Our expansion is a singular-perturbation expansion in this sense.

3 Formulation of the problem in parabolic coordinates

Consider a crystal, of initially parabolic shape, growing into an undercooled melt in two dimensions. Far from the solid-melt interface, the melt is assumed to be at temperature $T_\infty < T_M$, with T_M the melting temperature, while the solid is assumed to approach the temperature $\bar{T}$. Assume that the solid phase grows into the liquid in the positive z direction at a constant velocity V and that the solid and melt have molar specific heat and diffusivity, respectively, $C_p^{\pm}$, $D^{\pm}$, where + (−) refers to the liquid (solid) phases. Let L be the molar specific heat of solidification.

We introduce a coordinate system that is moving in the positive z direction with speed V with origin fixed at the tip. The location of the interface is expressed by the equation

$$\Phi(z,x,t) \equiv z - \zeta(x,t) = 0. \tag{1}$$

Defining the diffusive length scale $\ell = 2D^+/V$, replacing all lengths by dimensionless quantities in terms of ℓ, and scaling time by $2\ell/V$, we are led to the dimensionless system of equations for the temperature field

$$U^+ \to \Delta \quad , \quad z > \zeta(x,t), \begin{cases} z \to \infty \\ \text{or } |x| \to \infty \text{ , z fixed} \end{cases} \tag{2}$$

$$\triangle U^+ + 2\frac{\partial U^+}{\partial z} = \frac{\partial U^+}{\partial t} \quad , \quad z > \zeta(x,t) \tag{3}$$

$$\delta \triangle U^- + 2\frac{\partial U^-}{\partial z} = \frac{\partial U^-}{\partial t} \quad , \quad z < \zeta(x,t) \tag{4}$$

$$U^- \to \bar{\Delta} \quad , \quad z \to -\infty, \text{x fixed}, z < \zeta(x,t) \tag{5}$$

$$U^{\pm} = -\epsilon(1-\alpha\cos 4\theta)\mathcal{K} \qquad \text{on } z = \zeta(x,t) \tag{6}$$

$$\left[\vec{V}_\perp - \beta\nabla U^- + \nabla U^+\right]\cdot\vec{n} = 0 \qquad \text{on } z = \zeta(x,t). \tag{7}$$

Here we have introduced the quantities

$$U = \frac{C_p^+}{L}\left(T - T_M\right), \quad \beta = \frac{D^- C_p^-}{D^+ C_p^+}, \quad \epsilon = \frac{\gamma T_M C_p^+}{\ell L^2},$$
$$\Delta = \frac{C_p^+}{L}\left(T_\infty - T_M\right), \quad \bar{\Delta} = \frac{C_p^+}{L}\left(\bar{T} - T_M\right), \quad \delta = \frac{D^-}{D^+} \quad .$$

The ratio of capillary to diffusive lengths, ϵ, is a natural small parameter for our problem.

Of the two boundary conditions at the interface, (7) describes the energy balance there: the interface advances at a rate $(\mathbf{V}_\perp \cdot \mathbf{n})$ so that latent heat released is carried away by diffusion into both the solid and liquid phases. The other condition, (6), is the Gibbs–Thomson condition which asserts that the temperature at the interface is suppressed below T_M by capillary effects, by an amount proportional to the local curvature, $\mathcal{K} = \zeta_{xx}/\left[1 + (\zeta_x)^2\right]^{\frac{3}{2}}$. The other factor in (6), $(1 - \alpha\cos 4\theta)$, with θ the angle between the local normal and the z–direction, models the effects of crystalline anisotropy in the interfacial energy. Here a fourfold symmetry of the crystal is assumed [10], [1].

The shape of the crystal is assumed to be initially that of an Ivantsov parabola [8]. Following Horvay and Cahn [7], we introduce parabolic coordinates ξ and η defined by :

$$x = \xi\eta \quad , \quad z = \frac{\xi^2 - \eta^2}{2}. \tag{8}$$

Defining $\rho^2 = \xi^2 + \eta^2 = 2\sqrt{x^2 + z^2}$ we have

$$\nabla \;=\; \frac{1}{\rho}\left(\vec{e_\xi}\frac{\partial}{\partial\xi} + \vec{e_\eta}\frac{\partial}{\partial\eta}\right) \tag{9}$$

while the unit vectors in the two systems are related by

$$\vec{e_x} = \frac{1}{\rho}\left(\eta\vec{e_\xi} + \xi\vec{e_\eta}\right) \quad , \quad \vec{e_z} = \frac{1}{\rho}\left(\xi\vec{e_\xi} - \eta\vec{e_\eta}\right) \tag{10}$$

and

$$\vec{e_\xi} = \frac{1}{\rho}\left(\eta\vec{e_x} + \xi\vec{e_z}\right) \quad , \quad \vec{e_\eta} = \frac{1}{\rho}\left(\xi\vec{e_x} - \eta\vec{e_z}\right) \quad . \tag{11}$$

Throughout this discussion we have fixed a branch for our (double-valued) coordinate transformation by adopting $\xi \geq 0, \eta \cdot x \geq 0$. The fronts that we consider are nearly parabolic (typically of the form $\xi = A + \epsilon S(\eta, t, \epsilon)$). We assume that each can be described by

$$\xi = \Xi(\eta, t). \tag{12}$$

Then its unit normal $\vec{n}$ and curvature $\mathcal{K}$ are given by

$$\vec{n} \;=\; \frac{\vec{e_\xi} - \Xi_\eta\vec{e_\eta}}{\sqrt{1 + \Xi_\eta^2}}, \tag{13}$$

$$\mathcal{K}\left[\eta, \Xi(\eta, t)\right] \;=\; \frac{(\Xi - \eta\Xi_\eta)(1 + \Xi_\eta^2) - (\eta^2 + \Xi^2)\Xi_{\eta\eta}}{\left[(\eta^2 + \Xi^2)(1 + \Xi_\eta^2)\right]^{\frac{3}{2}}}, \tag{14}$$

while its normal velocity is

$$V_\perp = \vec{n} \cdot (2\vec{e_z} + \rho \Xi_t \vec{e_\xi}) \,. \tag{15}$$

The system (2-7), rewritten in parabolic coordinates, becomes

$$U^+ \to \Delta \quad , \quad \xi \to \infty \; , \; \eta \text{ fixed} \tag{16}$$

$$\left(\frac{\partial^2}{\partial \xi^2} + \frac{\partial^2}{\partial \eta^2}\right) U^+ + 2\left(\xi \frac{\partial}{\partial \xi} - \eta \frac{\partial}{\partial \eta}\right) U^+ = \rho^2 \frac{\partial U^+}{\partial t} \quad , \quad \xi > \Xi(\eta, t) \tag{17}$$

$$\delta \left(\frac{\partial^2}{\partial \xi^2} + \frac{\partial^2}{\partial \eta^2}\right) U^- + 2\left(\xi \frac{\partial}{\partial \xi} - \eta \frac{\partial}{\partial \eta}\right) U^- = \rho^2 \frac{\partial U^-}{\partial t} \quad , \quad \xi < \Xi(\eta, t) \tag{18}$$

$$U^- \to \bar{\Delta} \quad , \quad |\eta| \to \infty, \xi = 0 \tag{19}$$

$$2\left(\Xi + \eta \Xi_\eta\right) + (\eta^2 + \Xi^2)\Xi_t = \left(\frac{\partial}{\partial \xi} - \Xi_\eta \frac{\partial}{\partial \eta}\right)\left[\beta U^- - U^+\right] \quad , \quad \text{on} \;\; \xi = \Xi(\eta) \tag{20}$$

$$U^\pm = -\epsilon \left(1 - \alpha + \frac{8\alpha \left(\frac{-\eta + \Xi \Xi_\eta}{\Xi + \eta \Xi_\eta}\right)^2}{\left[1 + \left(\frac{-\eta + \Xi \Xi_\eta}{\Xi + \eta \Xi_\eta}\right)^2\right]^2}\right) \mathcal{K}[\eta, \Xi(\eta)] \quad , \quad \text{on} \;\; \xi = \Xi(\eta), \tag{21}$$

with $\mathcal{K}$ given by (14).

In the sequel we assume that the time scale governing the growth of the crystal is much slower than the time required by the temperature field to reach equilibrium (quasi-static approximation) so that the time derivatives in (17, 18) are neglected and the only time dependence in the problem enters through the energy balance (20).

4 Linearization for short times, with small surface tension

In this section we derive the equations for the evolution, under the influence of weak surface tension, of an interface that is initially close to an Ivantsov parabola. For $\epsilon << 1$, we assume that for short times, the interface and temperature fields have the form:

$$\begin{aligned} \Xi &= A + \epsilon S(\eta, t; \epsilon) && (22) \\ U^\pm &= U_I^\pm(\eta, \xi) + \epsilon u^\pm(\eta, \xi, t; \epsilon) && (23) \end{aligned}$$

where $\xi = A$ and $U_I^\pm$ are the Ivantsov interface and temperature field respectively. Consider expansions of the various equations in powers of ϵ. At leading order, the Gibbs-Thomson relation (21) gives

$$U_I^\pm = 0 \text{ at } \xi = A, \tag{24}$$

and at higher order

$$\left(S \frac{\partial U_I^\pm}{\partial \xi}(\eta, A) + u^\pm(\eta, A, t; \epsilon)\right) + \epsilon S \left\{\frac{S}{2} \frac{\partial^2 U_I^\pm}{\partial \xi^2}(\eta, A) + \frac{\partial u^\pm}{\partial \xi}(\eta, A, t; \epsilon)\right\} + \mathcal{O}(\epsilon^2)$$

$$= \frac{1}{(\eta^2+A^2)^{3/2}} \left[A + \epsilon \left\{ S - \frac{3SA^2}{\eta^2+A^2} - \eta S_\eta - (\eta^2+A^2) S_{\eta\eta} \right\} \right] \tag{25}$$
$$\left[1 - \alpha + \frac{8\alpha A^2 \eta^2}{(A^2+\eta^2)^2} - \frac{16\epsilon\alpha A\eta(A^2-\eta^2)}{(A^2+\eta^2)^3} \left\{ (A^2+\eta^2) S_\eta + \eta S \right\} \right] + \mathcal{O}(\epsilon^2)$$

We have retained higher order terms in (25) because we expect perturbations to develop high spatial derivatives and we specifically want to study their leading effects.

The equation of energy balance at the interface (20) becomes

$$\begin{aligned} &2A + \epsilon \left[2(S+\eta S_\eta) + (\eta^2+A^2) S_t + \epsilon 2ASS_t + \epsilon^2 S^2 S_t \right] \\ &= \quad \left(\frac{\partial}{\partial \xi} - \epsilon S_\eta \frac{\partial}{\partial \eta} \right) \left[\left(\beta U_I^- - U_I^+ \right) + \epsilon \left(\beta u^- - u^+ \right) \right] \Big|_{\xi = A+\epsilon S} . \end{aligned} \tag{26}$$

Expanding functions in Taylor series around the interface position we get at leading order

$$2A = \beta \frac{\partial U_I^-}{\partial \xi}(\eta, A) - \frac{\partial U_I^+}{\partial \xi}(\eta, A) \tag{27}$$

and at higher order

$$\begin{aligned} 2(S+\eta S_\eta) + (\eta^2+A^2) S_t \quad &+ \quad \epsilon \left(2ASS_t + \epsilon S^2 S_t \right) \quad = \\ \left[S \frac{\partial^2}{\partial \xi^2} - S_\eta \frac{\partial}{\partial \eta} \right. \quad &+ \quad \left. \epsilon \left(\frac{S^2}{2} \frac{\partial^3}{\partial \xi^3} - S S_\eta \frac{\partial^2}{\partial \xi \partial \eta} \right) \right] \left(\beta U_I^- - U_I^+ \right) \Big|_{\xi=A} \\ + \left[\frac{\partial}{\partial \xi} \right. \quad &+ \quad \left. \epsilon \left(S \frac{\partial^2}{\partial \xi^2} - S_\eta \frac{\partial}{\partial \eta} \right) \right] \left(\beta u^- - u^+ \right) \Big|_{\xi=A} + \mathcal{O}(\epsilon^2). \end{aligned} \tag{28}$$

We proceed now with the derivation of the zeroth-order (Ivantsov) solution. Collecting all expressions, we have that to $\mathcal{O}(1)$ the temperature satisfies:

$$U_I^+ \to \Delta < 0 \quad , \quad \xi \to \infty \tag{29}$$
$$\left(\frac{\partial^2}{\partial \xi^2} + \frac{\partial^2}{\partial \eta^2} \right) U^+ + 2 \left(\xi \frac{\partial}{\partial \xi} - \eta \frac{\partial}{\partial \eta} \right) U^+ = 0 \ , \ \xi > A \tag{30}$$
$$\delta \left(\frac{\partial^2}{\partial \xi^2} + \frac{\partial^2}{\partial \eta^2} \right) U^- + 2 \left(\xi \frac{\partial}{\partial \xi} - \eta \frac{\partial}{\partial \eta} \right) U^- = 0 \ , \ \xi < A \tag{31}$$
$$U_I^- \to \bar{\Delta} \quad , \quad |\eta| \to \infty, \xi = 0 \tag{32}$$
$$U_I^\pm = 0 \qquad \text{on } \xi = A \tag{33}$$
$$2A = \beta \frac{\partial U_I^-}{\partial \xi} - \frac{\partial U_I^+}{\partial \xi} \qquad \text{on } \xi = A. \tag{34}$$

The solution is found by separating variables to be:

$$U_I^+(\xi) = \Delta - C \int_\xi^\infty e^{-s^2} ds, \tag{35}$$
$$U_I^-(\xi) = \bar{\Delta} - \bar{C} \int_0^\xi e^{-s^2/\delta} ds, \tag{36}$$

where the constants $C, \bar{C}$ are determined from the boundary condition (33) to be

$$C = \frac{\Delta}{\int_A^\infty e^{-t^2} dt} \quad , \quad \bar{C} = \frac{\bar{\Delta}}{\int_0^A e^{-t^2/\delta} dt}. \tag{37}$$

Define the Peclet number to be

$$\mathcal{P} = A^2 \tag{38}$$

where A^2 is the dimensionless tip radius. Then (34) results in the relation:

$$\sqrt{\pi \mathcal{P}} e^{\mathcal{P}} erfc(\sqrt{\mathcal{P}}) = -\Delta - \frac{\beta \bar{\Delta} e^{\mathcal{P}(1-1/\delta)} erfc(\sqrt{\mathcal{P}})}{\sqrt{\delta} erf(\sqrt{\mathcal{P}/\delta})} \tag{39}$$

in which the error function, $erf(z)$, and complementary error function, $erfc(z)$, are defined as usual:

$$erf(z) = \frac{2}{\sqrt{\pi}} \int_0^z e^{-t^2} dt, \quad erfc(z) = \frac{2}{\sqrt{\pi}} \int_z^\infty e^{-t^2} dt \quad .$$

Relation (39) was first derived by Ivantsov ([8]) with $\bar{\Delta} = 0$.

At this point we assume that the various thermal coefficients for the solid and melt phases are the same and that the solid is kept at the freezing temperature at ∞, so that

$$\delta = 1 \quad , \quad \bar{\Delta} = 0 \quad , \quad \beta = 1.$$

Under these assumptions

$$\left.\frac{\partial U_I^+}{\partial \xi}\right|_A = -2\sqrt{\mathcal{P}} \ , \quad \left.\frac{\partial^2 U_I^+}{\partial \xi^2}\right|_A = 4\mathcal{P} \ , \quad \left.\frac{\partial U_I^-}{\partial \xi}\right|_A = \left.\frac{\partial^2 U_I^-}{\partial \xi^2}\right|_A = 0. \tag{40}$$

We now obtain the equations for the perturbation ($u^\pm$, S) at leading order as $\epsilon \to 0$. Using (40) we have

$$\begin{aligned}
\left(\frac{\partial^2}{\partial \xi^2} + \frac{\partial^2}{\partial \eta^2}\right) u^+ \ &+ \ 2\left(\xi \frac{\partial}{\partial \xi} - \eta \frac{\partial}{\partial \eta}\right) u^+ = 0 \ , \ \xi < A &(41)\\
\left(\frac{\partial^2}{\partial \xi^2} + \frac{\partial^2}{\partial \eta^2}\right) u^- \ &+ \ 2\left(\xi \frac{\partial}{\partial \xi} - \eta \frac{\partial}{\partial \eta}\right) u^- = 0 \ , \ \xi > A &(42)\\
u^+(\eta, \sqrt{\mathcal{P}}, t) - 2\sqrt{\mathcal{P}} S \ &= \ u^-(\eta, \sqrt{\mathcal{P}}, t) &(43)\\
&= \ \frac{\sqrt{\mathcal{P}} - \epsilon(\eta^2 + \mathcal{P}) S_{\eta\eta}}{(\eta^2 + \mathcal{P})^{3/2}} \left[1 - \alpha + \frac{8\alpha \mathcal{P} \eta^2}{(\mathcal{P} + \eta^2)^2}\right] + \mathcal{O}(\epsilon^2) &\\
2(S + \eta S_\eta) + (\eta^2 + \mathcal{P}) S_t \ &= \ -4\mathcal{P} S + \epsilon \sqrt{\mathcal{P}}(4\mathcal{P} - 2) S^2 &(44)\\
&+ \ \left(\frac{\partial}{\partial \xi} + \epsilon S \frac{\partial^2}{\partial \xi^2} - \epsilon S_\eta \frac{\partial}{\partial \eta}\right) \left(u^- - u^+\right)\Big|_{\xi = \sqrt{\mathcal{P}}} + \mathcal{O}(\epsilon^2). &
\end{aligned}$$

For solutions of (41–44) that are $\mathcal{O}(1)$ and whose derivatives are also $\mathcal{O}(1)$, leading order effects can be obtained simply by setting $\epsilon = 0$ in (43, 44). However, (41–44) also admit highly oscillatory solutions in which $S = \mathcal{O}(1)$, $\epsilon S_{\eta\eta} = \mathcal{O}(1)$, even though $\epsilon << 1$. For those highly oscillatory solutions we must retain the highest derivative term in (43), $\epsilon S_{\eta\eta}$, even for $\epsilon \to 0$. Thus the small ϵ expansion is a singular perturbation expansion, as had been anticipated by Langer and Müller–Krumbhaar [13]. It follows from (41, 42) that if $\dfrac{\partial}{\partial\eta} = \mathcal{O}(\epsilon^{-1/2})$ then $\dfrac{\partial}{\partial\xi} = \mathcal{O}(\epsilon^{-1/2})$ as well. Then estimates of the nominally small terms at (44) indicate that they all remain small in the limit in which the extra term in (43) becomes important: $\partial_\eta = \mathcal{O}(\epsilon^{-1/2})$, $\partial_\xi = \mathcal{O}(\epsilon^{-1/2})$ as $\epsilon \to 0$. To summarize, the small ϵ limit of (41–44) is obtained by retaining the term $\epsilon S_{\eta\eta}$ in (43) and letting $\epsilon \to 0$ elsewhere.

The Laplace equation (41, 42) is separable in parabolic coordinates [18]. Assuming for the temperature fields and interface deformation the expansions

$$\begin{aligned} u^{\pm} &= \sum_{j=0}^{\infty} W_j^{\pm}(t) H_j(\eta) F_j^{\pm}(\xi), &(45)\\ S(\eta,t;\epsilon) &= \sum_{j=0}^{\infty} S_j(t) H_j(\eta). &(46)\end{aligned}$$

(where the coefficients S_j, W_j also depend on $\mathcal{P}$, ϵ and α), we find

$$H_j'' - 2\eta H_j' + 2jH_j = 0, \tag{47}$$
$$F_j'' + 2\xi F_j' - 2jF_j = 0. \tag{48}$$

The first of these is the Hermite equation, in which requiring H_j to be real and to grow no worse than algebraically at infinity results in j being a nonnegative integer ([14]):

$$\begin{aligned} H_j(\eta) &= (-1)^j e^{\eta^2} \frac{d^j e^{-\eta^2}}{d\eta^j},\ j = 0,1,2,\ldots &(49)\\ \text{with } \int_{-\infty}^{\infty} e^{-x^2} H_n H_m dx &= \delta_{mn} 2^n n! \sqrt{\pi} \equiv \delta_{mn} c_n. &(50)\end{aligned}$$

Also, requiring that F_j^+ grow no worse than algebraically at infinity and that F_j^- and $F_j^{-\prime}$ be continuous at $\xi = 0$ results in the following expressions for $F_j^{\pm}$:

$$F_j^-(\xi) = \begin{cases} \sum_{k=0}^{m} a_{2k}^j \xi^{2k},\ j = 2m \\ \sum_{k=0}^{m} a_{2k+1}^j \xi^{2k+1},\ j = 2m+1 \end{cases} \tag{51}$$

$$\text{with } a_{k+2}^j = \frac{2(j-k)}{(k+2)(k+1)} a_k^j \quad , \quad a_1^{2j+1} = a_0^{2j} \quad , \quad a_0^{2j+2} = \frac{a_0^{2j}}{4(j+1)}$$

$$F_j^+(\xi) = \int_{\xi}^{\infty} e^{-s^2} \frac{(s-\xi)^j}{j!} ds. \tag{52}$$

For future reference, it is convenient to introduce

$$F_{-1}^- \equiv 0,\ F_{-1}^+(A) \equiv -e^{-A^2}, \tag{53}$$

and to note that the functions $F_j^{\pm}$, H_j satisfy the recursions:

$$F_j^{\pm\prime} = \mp F_{j-1}^{\pm} \tag{54}$$

$$F_{j-2}^{\pm} \mp 2\xi F_{j-1}^{\pm} - 2jF_j^{\pm} = 0 \tag{55}$$

$$H_j' = 2jH_{j-1} \tag{56}$$

$$2jH_{j-1} - 2\eta H_j + H_{j+1} = 0 \quad . \tag{57}$$

It is well-known [14] that series of the form (45, 46) can be used to represent functions with quite general growth behaviour as $\eta \to \infty$. In fact, for a function $S(\eta)$ on the infinite interval $(-\infty, \infty)$ which is piecewise smooth on any finite subinterval and such that

$$\int_{-\infty}^{\infty} e^{-\eta^2} S^2(\eta) d\eta < \infty, \tag{58}$$

the expansion (46) with coefficients

$$S_j = \frac{1}{c_j} \int_{-\infty}^{\infty} e^{-\eta^2} H_j(\eta) S(\eta) d\eta$$

converges at each point to the value $1/2(S(\eta+) + S(\eta-))$. The broad class of interfacial shapes allowed by (58) is one of the main advantages of using a parabolic coordinate system.

Turning now to the perturbed Gibbs–Thomson relation (43), we define two sets of coefficients, $\sigma_{2k}(\mathcal{P}, \alpha)$ and $f_j(\mathcal{P}, \alpha)$ by

$$\frac{1}{(\eta^2 + \mathcal{P})^{3/2}} \left[1 - \alpha + \frac{8\alpha \mathcal{P} \eta^2}{(\mathcal{P} + \eta^2)^2} \right] \stackrel{\text{def}}{=} \sum_{k=0}^{\infty} \sigma_{2k}(\mathcal{P}; \alpha) H_{2k}(\eta) \tag{59}$$

and

$$\frac{S_{\eta\eta}}{(\eta^2 + \mathcal{P})^{1/2}} \left[1 - \alpha + \frac{8\alpha \mathcal{P} \eta^2}{(\mathcal{P} + \eta^2)^2} \right] \equiv \sum_{j=0}^{\infty} f_j(\mathcal{P}, \alpha) H_j. \tag{60}$$

Note that $\sigma_{2k+1} \equiv 0, k = 0, 1, \cdots$ as we are expanding an even function. Substituting the above expansions to (43) yields

$$\begin{aligned} \sum_{j=0}^{\infty} [\sqrt{\mathcal{P}} \sigma_j(\mathcal{P}; \alpha)] H_j - \epsilon \sum_{j=0}^{\infty} f_j H_j &= \sum_{j=0}^{\infty} [W_j^+ F_j^+(A)] H_j - 2\sqrt{\mathcal{P}} \sum_{j=0}^{\infty} S_j H_j \\ &= \sum_{j=0}^{\infty} [W_j^- F_j^-(A)] H_j \end{aligned}$$

and solving for $W_j^{\pm}$ we find:

$$W_j^+ = \left[\frac{\sqrt{\mathcal{P}} \sigma_j(\mathcal{P}; \alpha)}{F_j^+(A)} \right] + \left[\frac{2\sqrt{\mathcal{P}}}{F_j^+(A)} \right] S_j - \left[\frac{\epsilon}{F_j^+(A)} \right] f_j(\mathcal{P}, \alpha),$$

$$W_j^- = \left[\frac{\sqrt{\mathcal{P}}\sigma_j(\mathcal{P};\alpha)}{F_j^-(A)}\right] - \left[\frac{\epsilon}{F_j^-(A)}\right] f_j(\mathcal{P},\alpha).$$

Turning now to (44) we use the following identities:

$$\begin{aligned}\eta S = \sum_{j=0}^{\infty} S_j[\frac{1}{2}H_{j+1} + jH_{j-1}] \quad &= \quad \sum_{j=0}^{\infty}[\frac{1}{2}S_{j-1} + (j+1)S_{j+1}]H_j \\ &\quad\; S_{-1} \equiv \; S_{-2} \equiv 0\end{aligned}$$

so that

$$\eta S_\eta = \sum_{j=0}^{\infty}[jS_j]H_j + \sum_{j=0}^{\infty}[2(j+1)(j+2)S_{j+2}]H_j \tag{61}$$

and

$$(\eta^2 + \mathcal{P})S_t \;=\; \sum_{j=0}^{\infty}[\frac{1}{4}S'_{j-2} + \left(j + \mathcal{P} + \frac{1}{2}\right) S'_j + (j+2)(j+1)S'_{j+2}]H_j$$

with

$$S_t = \sum_{j=0}^{\infty} S'_j H_j.$$

Also,

$$\frac{\partial}{\partial \xi}u^{\pm}\bigg|_{\sqrt{\mathcal{P}}} = \sum_{j=0}^{\infty} W_j^{\pm} F_j^{\pm'}(A) H_j$$

and using the relations (54) we have

$$\frac{\partial}{\partial \xi}(u^- - u^+)\bigg|_{\sqrt{\mathcal{P}}} = \sum_{j=0}^{\infty}\{W_j^- F_{j-1}^-(A) + W_j^+ F_{j-1}^+(A)\}H_j$$

where we have used (53). We now substitute the expressions derived above into (44), to get

$$\begin{aligned} & \sum_{j=0}^{\infty}(2S_j)H_j + 2\sum_{j=0}^{\infty}[jS_j + 2(j+1)(j+2)S_{j+2}]H_j \\ + \quad & \sum_{j=0}^{\infty}\left[\frac{1}{4}S'_{j-2} + (j + \mathcal{P} + \frac{1}{2})S'_j + (j+1)(j+2)S'_{j+2}\right] H_j \\ = \quad & \sum_{j=0}^{\infty}\Big\{W_j^- F_{j-1}^-(A) + W_j^+ F_{j-1}^+(A)\Big\}H_j - 4\mathcal{P}\sum_{j=0}^{\infty} S_j H_j. \end{aligned}$$

Here, the first two lines give the latent heat release from the basic motion of the parabolic front, due to the shape perturbations. The first term of the third line gives the flux of the perturbation field at the parabola, while the second term gives the flux of the leading field at the perturbed interface.

Collecting results, we finally get the system of equations, for $j = 0, 1, 2, \cdots$:

$$\begin{aligned} & \frac{1}{4}S'_{j-2} + (j + \mathcal{P} + \frac{1}{2})S'_j + (j+1)(j+2)S'_{j+2} \\ + \quad & 2(j + 1 + 2\mathcal{P}\tau_j^+(A))S_j + 4(j+1)(j+2)S_{j+2} \\ = \quad & 2\mathcal{P}(\tau_j^- - \tau_j^+)\sigma_j(\mathcal{P};\alpha) - 2\epsilon\sqrt{\mathcal{P}}(\tau_j^- - \tau_j^+)f_j(\mathcal{P},\alpha), \end{aligned} \tag{62}$$

where $S_{-2} = S_{-1} = 0$, and the coefficients $\tau_j^\pm$ are defined by:

$$\tau_j^\pm = 1 \mp \frac{1}{2\sqrt{\mathcal{P}}}\frac{F_{j-1}^\pm(A)}{F_j^\pm(A)}. \tag{63}$$

Our analysis centers on system (62). It gives the evolution of perturbations to the parabolic shape of the front, in terms of the coefficients in the Hermite expansion of the shape perturbations. Our work is based on the hypothesis that if a selection mechanism exists, it must be possible to find it by studying the spectrum of this system as the controlling parameters ($\mathcal{P}$, ϵ, α) are varied, as well as the behavior of the unstable modes near the tip.

The $F_j^\pm$ are solutions of (48) but it is not necessary to solve such equations separately in order to determine the $\tau_j^\pm$. Indeed, by using the recursions (55) we see that

$$\tau_j^\pm = 1 + \frac{j}{2\mathcal{P}}\frac{1}{\tau_{j-1}^\pm} \tag{64}$$

which, together with the relations

$$\tau_0^+ = 1 - \frac{e^{-\mathcal{P}}}{2\sqrt{\mathcal{P}}\int_{\sqrt{\mathcal{P}}}^\infty e^{-s^2}ds} \quad , \quad \tau_0^- = 1 \tag{65}$$

give complete recursion sequences that determines the coefficients $\tau_j^\pm$.

5 Analogue of the Mullins–Sekerka instability

The system of equations in (62) contains a great deal of information about the evolution in two dimensions of nearly parabolic fronts under the influence of weak surface tension, with or without crystalline anisotropy. Here are three kinds of information available from (62):
(a) Neglecting all time derivatives in the first line of (62) results in a set of nonhomogeneous, algebraic equations for the Hermite coefficients S_j of the steady-state shape of the perturbed interface, in the presence of nonzero surface tension. These steady shapes might or might not be dynamically stable.
(b) Neglecting the nonhomogeneous terms σ_j in the last line of (62) provides a linear, homogeneous system of differential equations for the shape of a growing interface. The family of solutions of these equations provides the analogue, on a parabolic interface, of the Mullins–Sekerka instability on a flat interface. This analogy is limited by the fact that the derivation

of (62) required small surface tension ($\epsilon << 1$), whereas the original analysis of Mullins and Sekerka [19] was not restricted in this way.
(c) Having computed the time-dependent growth of the unstable modes of (62) for a particular Ivantsov parabola, one implements the dynamic selection criterion proposed in Section 2 by determining whether these growing modes leave quiescent a neighborhood of the tip of the growing crystal.

We develop now some notation for the study of system (62). We define $\mathbf{M}$ to be the operator of multiplication by η^2 and we let $\mathbf{N} = \mathbf{M} + \mathcal{P}\mathbf{I}$. The form of $\mathbf{N}$ is seen in the first line of (62). We also define the matrix $\mathbf{K}$ to be the Hermite representation of the operator $2 + 2\eta\dfrac{d}{d\eta} + 4\mathcal{P}\mathbf{T}^{+}$, given in the second line of (62) with $T^{+}_{ij} = \tau^{+}_{j}\delta_{ij}$. Finally we let $\mathbf{T}$ be the diagonal matrix with elements $T_j = \tau^{-}_{j} - \tau^{+}_{j}$, and $\mathbf{U}$ a matrix with only the second superdiagonal different from zero, and whose $(j, j+2)$ element is $U_{j,j+2} = 4(j+1)(j+2)$. Then, (62) can be written as

$$\mathbf{N}S' + \mathbf{K}S = 2\mathcal{P}\mathbf{T}\Sigma - 2\epsilon\sqrt{\mathcal{P}}\mathbf{T}F. \tag{66}$$

For the isotropic case, $\alpha = 0$. We introduce the symmetric matrix G_{mn} by writing

$$\begin{aligned} f_j(\mathcal{P}, 0) &= \frac{1}{c_j}\int_{-\infty}^{\infty} e^{-\eta^2}\frac{S_{\eta\eta}}{\sqrt{\eta^2+\mathcal{P}}}H_j(\eta)d\eta \\ &= \frac{4}{c_j}\sum_{l=0}^{\infty}(l+1)(l+2)S_{l+2}\int_{-\infty}^{\infty} e^{-\eta^2}\frac{H_l(\eta)H_j(\eta)}{\sqrt{\eta^2+\mathcal{P}}}d\eta \\ &= \frac{4}{c_j}\sum_{l=0}^{\infty}(l+1)(l+2)S_{l+2}G_{jl} = \frac{1}{c_j}\sum_{l,m=0}^{\infty} G_{jl}U_{lm}S_m, \end{aligned} \tag{67}$$

with the c_j defined in (50). The coefficients f_j, G_{mn} (as well as the $\tau^{\pm}_{j}$ of the previous section) can be found through recursions. These computations turn out to be quite involved numerically (due to the presence of undesired dominant solutions of the recursions) but a suitable use of asymptotics allows the determination of these coefficients to arbitrary accuracy. This computation will be presented in detail elsewhere.

For $\alpha \neq 0$ it follows from (60) that $\mathbf{N}^2 F = \mathbf{C}^{-1}\left((1-\alpha)\mathbf{N}^2 + 8\mathcal{P}\alpha\mathbf{M}\right)\mathbf{G}\mathbf{U}S$, so that (66) becomes

$$\mathbf{N}^2\mathbf{T}^{-1}(\mathbf{N}S' + \mathbf{K}S) - 2\mathcal{P}\mathbf{N}^2\Sigma = -2\epsilon\sqrt{\mathcal{P}}\left((1-\alpha)\mathbf{N}^2 + 8\mathcal{P}\alpha\mathbf{M}\right)\mathbf{C}^{-1}\mathbf{G}\mathbf{U}S, \tag{68}$$

with $C_{ij} = c_i\delta_{ij}$. The latter form allows a computation for the anisotropic case to be performed with no additional complexity compared to the isotropic case.

Now we restrict attention to the isotropic case, $\alpha = 0$. For our actual computations, it proved beneficial to introduce a new scaling, in terms of orthonormal Hermite polynomials. Thus, we rescale the Hermite coefficients S_j as $\hat{S} = \mathbf{\Lambda}S$ with $\Lambda_{ij} = \delta_{ij}\sqrt{2^j j!}$. Then, equation (68) becomes

$$\begin{aligned} &\mathbf{\Lambda}\mathbf{N}\mathbf{\Lambda}^{-1}\mathbf{\Lambda}S' + \mathbf{\Lambda}\mathbf{K}\mathbf{\Lambda}^{-1}\mathbf{\Lambda}S - 2\mathcal{P}\mathbf{T}\mathbf{\Lambda}\Sigma \\ &= -2\epsilon\sqrt{\mathcal{P}}\mathbf{T}\mathbf{C}^{-1}\mathbf{\Lambda}\mathbf{G}\mathbf{\Lambda}^{-1}\mathbf{\Lambda}\mathbf{U}\mathbf{\Lambda}^{-1}\mathbf{\Lambda}S. \end{aligned} \tag{69}$$

We note that the matrix $\hat{\mathbf{N}} = \mathbf{\Lambda N \Lambda}^{-1}$ is symmetric, with main diagonal same as that of $\mathbf{N}$ (i.e. $N_j = \hat{N}_{jj} = (j + \mathcal{P} + 1/2)$), and with second super– and subdiagonals equal to $(\hat{N}_{j,j+2} = \hat{N}_{j+2,j} =)(1/2)\sqrt{(j+1)(j+2)}$. Similarly the matrix $\hat{\mathbf{K}} = \mathbf{\Lambda K \Lambda^{-1}}$ has nonzero elements $\hat{K}_{jj} = K_{jj} = 2(j + 1 + 2\mathcal{P}\tau_j^+)$ and $\hat{K}_{j,j+2} = 2\sqrt{(j+1)(j+2)}$.

Also, $\hat{\mathbf{G}} = \mathbf{C}^{-1}\mathbf{\Lambda G \Lambda}^{-1}$ is given by

$$(\hat{G})_{ij} = \frac{\sqrt{2^i i!}}{c_i} G_{ij} \frac{1}{\sqrt{2^j j!}} = \frac{1}{\sqrt{\pi}} \frac{G_{ij}}{\sqrt{2^{i+j} i! j!}}$$

while $\hat{\mathbf{U}} = \mathbf{\Lambda U \Lambda}^{-1}$ is a matrix of zeroes except for the $(j, j+2)$ diagonal which contains

$$(\hat{U})_{j,j+2} = 2\sqrt{(j+1)(j+2)}.$$

Now we focus on the homogeneous problem associated with (66), in order to study the analogue of the Mullins-Sekerka instability on a parabolic interface. The homogeneous problem can be formulated as a generalized eigenvalue problem: assuming that $\hat{S}_j(t)$ has the form $\hat{S}_j(t) = s_j e^{\lambda t}$ we have the eigensystem

$$\lambda \hat{\mathbf{N}} s + \hat{\mathbf{K}} s = -2\epsilon\sqrt{\mathcal{P}}\mathbf{T}\hat{\mathbf{G}}\hat{\mathbf{U}} s$$

or

$$\lambda \hat{\mathbf{N}} s = -\left(\hat{\mathbf{K}} + 4\epsilon\sqrt{\mathcal{P}}\mathbf{B}\right) s, \tag{70}$$

where we have introduced $\mathbf{B} = \frac{1}{2}\mathbf{T}\hat{\mathbf{G}}\hat{\mathbf{U}}$. The matrix elements of $\mathbf{B}$ are

$$\begin{aligned} B_{ij} &= \frac{1}{2} T_{il} \hat{G}_{ln} \hat{U}_{nj} \quad \text{(sum over repeated indices)} \\ &= \frac{1}{2} T_{ii} \hat{G}_{i,j-2} \hat{U}_{j-2,j} \quad \text{(no sums)} \\ &= (\tau_i^- - \tau_i^+)\sqrt{j(j-1)}\hat{G}_{i,j-2} \quad , \quad j = 2, 3, \cdots \\ & \quad \text{with} \quad B_{i,0} = B_{i,1} = 0 \quad , \quad i = 1, 2, \cdots \end{aligned}$$

Note that in this system even and odd modes uncouple, effectively doubling the size of any truncation. Thus all our computations were performed on purely even or odd mode truncations, and the term "order of truncation" is used to denote the number of even or odd modes actually used.

We present now some preliminary results that were obtained from our computations of the spectrum of the system (70) with small, but nonzero, ϵ. An approach that we found satisfactory in computing the spectrum utilizes the fact that (70) is in the standard form for the QZ–factorization algorithm of Moler and Stewart [17] to be applicable. We used the EISPACK generalized eigenvalue solver which allowed us to compute eigenvalues for truncations including up to 1600 even or odd modes. It was found by various comparisons that above truncations of order $500 - 700$, roundoff contamination was appreciable. In our computations with $\epsilon = 0$ we found that we could readily identify eigenvalues that stabilize, i.e. remain unchanged to a given tolerance over several truncations and discard the rest. For given $\mathcal{P}$, after increasing the truncation above a certain limit, roundoff prevented any further stabilized eigenvalues to appear.

For any ϵ in the range $0 \leq \epsilon \leq .01$ for which we have carried out computations, most of the computed spectrum of the truncated system was composed of eigenvalues lying, roughly, on two arcs (Figs. 1, 2). The outer arc, horse-shoe shaped for $\epsilon = 0$, becomes wider as the truncation increases and is apparently composed entirely of "spurious" eigenvalues, or eigenvalues of the truncated system that do not correspond to eigenvalues of the full system. The second, bell-shaped arc spans the horseshoe and is composed of eigenvalues that, once they appear, quickly settle to values that change very little as the order of truncation is increased.

However, without surface tension, ($\epsilon = 0$), system (70) is ill-posed with the growth rate of the instability being an increasing function of the wavenumber. In this limit of vanishing surface tension, the only correction to eq. (62) enters through the nonhomogeneous term, modifying smoothly the steady shape of the Ivantsov parabola, proportionally to the surface tension. Since instability ensues for any $\mathcal{P}$, this nearly parabolic profile is always unstable.

For any ϵ arbitrarily small but finite there exists a sufficiently high mode number for which the term

$$2\epsilon\sqrt{\mathcal{P}}(\tau_j^- - \tau_j^+)f_j(A)$$

becomes important. This term makes our eigenvalue problem well-posed for $\epsilon > 0$, introducing an upper frequency cutoff. We performed calculations for $\mathcal{P} = 2, 4$ and for truncations spanning the range 300 to 1600. For values of $\epsilon < .007$, only a part of the spectrum lies in the positive real half-plane, with nonzero lower wavenumber/frequency cutoffs (as well as an upper cutoffs for any $\epsilon > 0$, see Figs. 1, 2). The eigenfunctions corresponding to eigenvalues with positive real part appear as waves of constant phase velocity, traveling down the sides of the parabola. Some of the unstable eigenmodes are strongly localized away from the tip. As an example of such a localized eigenmode, for $\mathcal{P} = 4$, $\epsilon = .001$, the real part of the mode corresponding to the eigenvalue $\lambda = 3.926 \pm i7.534$ is shown in Fig. 3. Clearly this localized mode has an effective wavelength. We can use these effective wavelengths to compute phase velocities and dispersion curves.

We found that if the surface tension were chosen sufficiently high, the real parts of all the computed eigenvalues invariably became negative and the instability was suppressed. For $\mathcal{P} = 4$ and for $\epsilon > .007$ the spectrum lies entirely on the left half plane and no instability was found, as shown in Fig. 4.

For $\epsilon \neq 0$ however small, both arcs become bow-shaped and eventually they bend back to recross the imaginary axis. In (Figs. 1, 2) we give the spectra corresponding to even and odd eigenmodes, respectively, for $\mathcal{P} = 4$ and $\epsilon = .005$ for a truncation of order 512. As mentioned before, the "outer" arc (squares) does not settle but keeps changing shape as the order of truncation increase, while the "inner" arc (circles) simply elongates as truncation is increased and new eigenvalues appear, without changing shape. It appears that the computation for

$\epsilon \neq 0$ becomes much more sensitive to roundoff errors as compared to the case $\epsilon = 0$, so that for the truncations we considered and with 16 decimal digit arithmetic, individual eigenvalues did not settle quite satisfactorily. However the arc they define did settle, as can be seen in Fig. 5 where the computed spectrum for even eigenmodes at $\mathcal{P} = 4$, $\epsilon = .001$ is shown for trucations $M = 444$ (squares) and $M = 512$ (circles), superimposed for comparison, with the spurious part of the spectrum omitted. In Fig. 4, (with $\epsilon = .007$), as well as in Figs. 1, 2, a number of values shown that lie on neither arc should be attributed to roundoff contamination. The results were also found to be quite sensitive to the accuracy by which various coefficients in (70) were known. Considerable care was required in employing techniques for the computation of these coefficients that gave them to the maximum accuracy of 16 digits employed in the rest of the computations.

In conclusion, we present a comparison of our preliminary findings with previous studies of dendritic growth. The analysis of Mullins and Sekerka [19] for the instability of a flat solidification front shows both similarities and differences from our anlysis of a parabolic front, due to inherent physical differences in the two processes. The main points are:

1. The flat front corresponds to $\mathcal{P} \to \infty$, while a parabolic front can be found for every positive finite value of $\mathcal{P}$.

2. On a parabolic front, we find that each of the unstable modes, like the one shown in Fig. 3, has an effective wavenumber ($k \geq 0$), that $|\Im\lambda|$ increases as k increases, and $|\Im\lambda| \to 0$ as $k \to 0$. Therefore, a comparison is possible between the findings for the spectrum of the parabolic case and that for the flat case which has fourier modes, and for which typical stability diagrams are given as relations between k and $\Re\lambda$ ([12]).

3. Both cases show a cutoff for large k; that is, disturbances with sufficiently small wavelengths decay in either geometry.

4. For k small ($\Im\lambda$ small), $\Re\lambda < 0$, which differs from the flat interface case.

5. At least for $\mathcal{P} = 2$ and $\mathcal{P} = 4$, the instability is apparently suppressed for sufficiently large surface tension.

6. It is inappropriate to apply the known results from a flat interface to the sides of a parabola (where the interfacial curvature approaches zero). Along the sides of a parabola we must take into account the tangential motion of the liquid phase, which is not present at the flat interface.

In order to compare our findings with the results of other approaches to the dendritic growth problem, such as those of microscopic solvability, we still need to analyze the behavior of the steady correction to the front as $\eta \to \infty$. This analysis will be reported elsewhere.

Acknowledgements

E.C. wishes to acknowledge the hospitality and the use of the computing facilities at Risø National Laboratory, Denmark. H.S. was partially supported by NSF grant # DMS-9096156. Charles Troup (UNM) helped with the graphics. Bruce Fast (CU) provided logistics and systems help. Some of the preliminary computations were done at the NCSA's Cray-YMP. Funding for the final calculations on the Cray2 at Kirtland Air Force base, was provided by AFOSR.

References

[1] A. Barbieri, D.C. Hong and J. Langer, Phys. Rev. A 35, (1988), 1801.

[2] M. Ben-Amar and Y. Pomeau, Europhys. Lett., 2, 307, (1986).

[3] B. Caroli, C. Caroli, B. Roulet and C. Misbah, J. Physique, 48, 547, (1987).

[4] A. Dougherty, P. D. Kaplan and J. P. Gollub, Phys. Rev. Lett. 58, (1987), 1652-1655.

[5] M. E. Glicksman, in *Crystal growth of electronic materials*, E. Kaldis, ed., pp 57-69, Elsevier Sci. Pub. B. V., 1985.

[6] J.P. Gollub, these Proceedings.

[7] G. Horvay and J. W. Cahn, Acta Metal. 9, (1961), 695-705.

[8] G. P. Ivantsov, Dokl. Acad. Nauk SSSR 58, (1947), 567.

[9] D.A. Kessler, these Proceedings.

[10] D.A. Kessler, J. Koplik and H. Levine, Adv. in Phys. 37, (1988), 255–336.

[11] D.A. Kessler and H. Levine, Phys. Rev. B 33, 7687, (1986).

[12] J. S. Langer, Rev. Mod. Phys. 52, (1980), 1-28.

[13] J.S. Langer and H. Müller-Krumbhaar, Acta Metall. 26, 1681–1687, (1978); (Ibid), 1689-1695; (Ibid), 1697–1708.

[14] N.N. Lebedev, *Special Functions and their Applications*, Dover, NY (1972).

[15] H. Levine, these Proceedings.

[16] D. Meiron, Phys. Rev. A 33, 2704, (1986).

[17] C. Moler and Stewart, SIAM J. Num. Anal., 10, 241–256, (1973).

[18] P.M. Morse and H. Feshbach, Methods of Theoretical Physics, Vol. 1, McGraw-Hill, NY 1953.

[19] W.W. Mullins and R.F. Sekerka, J. Appl. Phys. 34, 444 (1964). 58, (1987),1652-1655.

[20] Y. Saito, G. Goldbeck-Wood and H. Müller-Krumbhaar, Phys. Rev. A 38, (1988), 2148-2157.

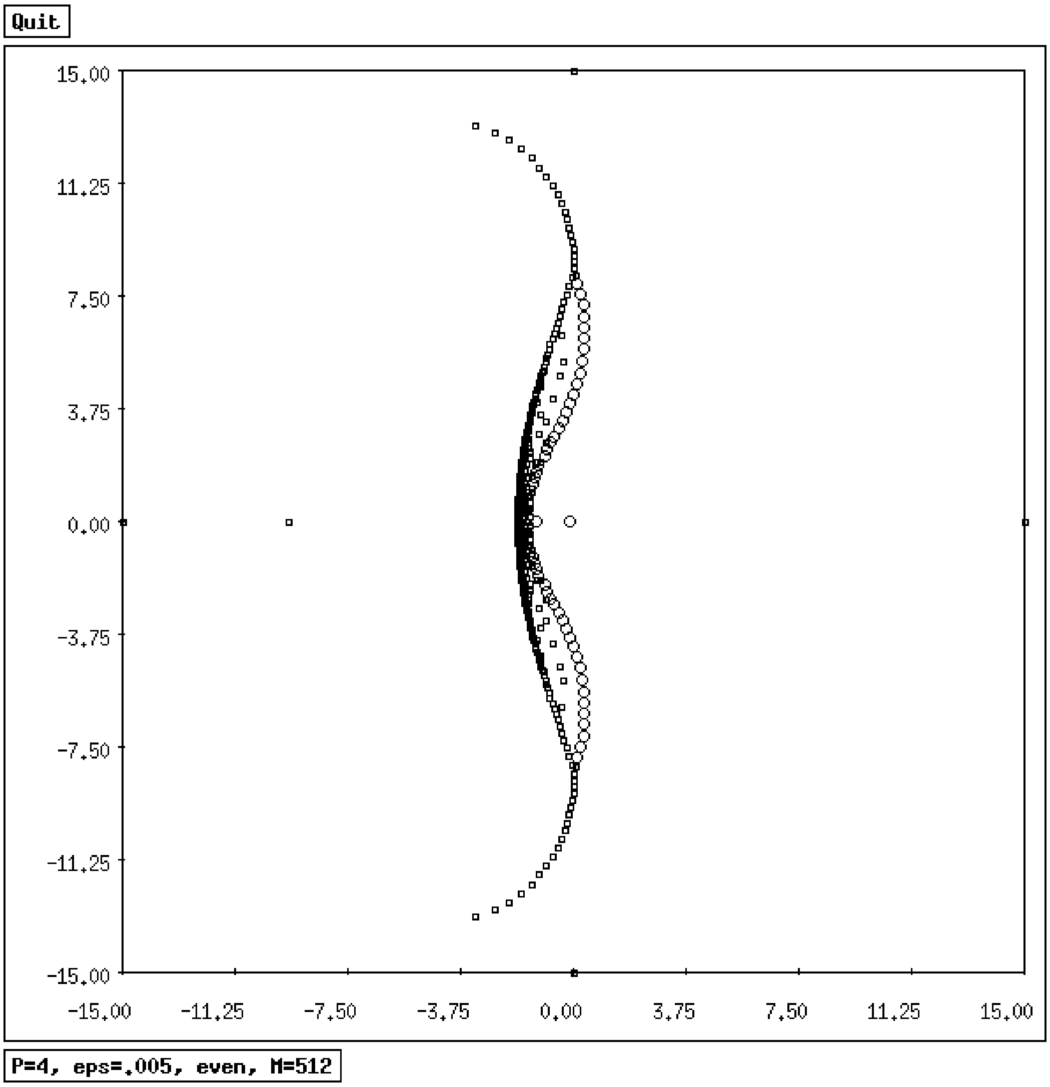

Figure 1: The spectrum for $Pe = 4$, $M = 512$ (even), $\epsilon = .005$. Eigenvalues on the stabilized arc are represented by circles, spurious eigenvalues by squares.

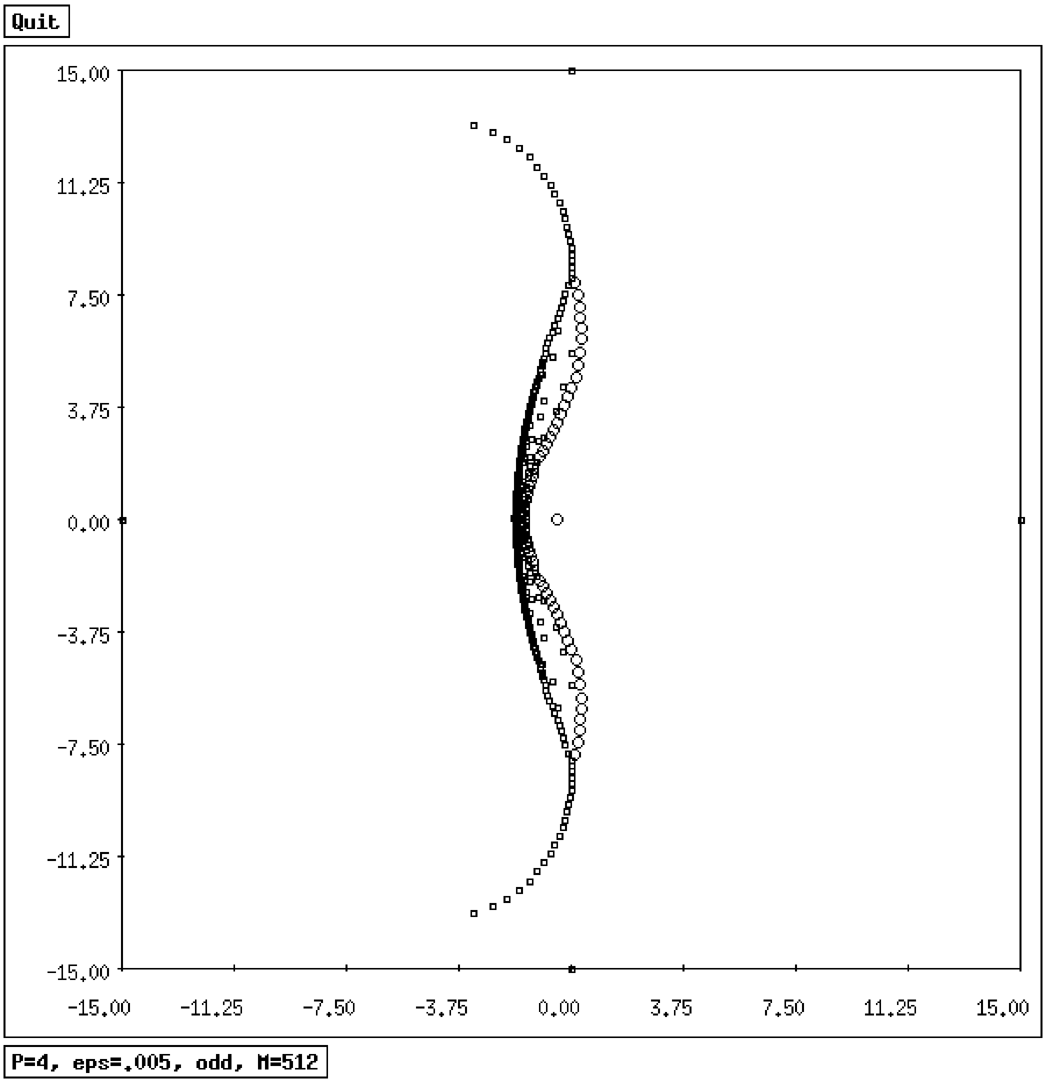

Figure 2: Same as in Fig. 1, for odd truncation.

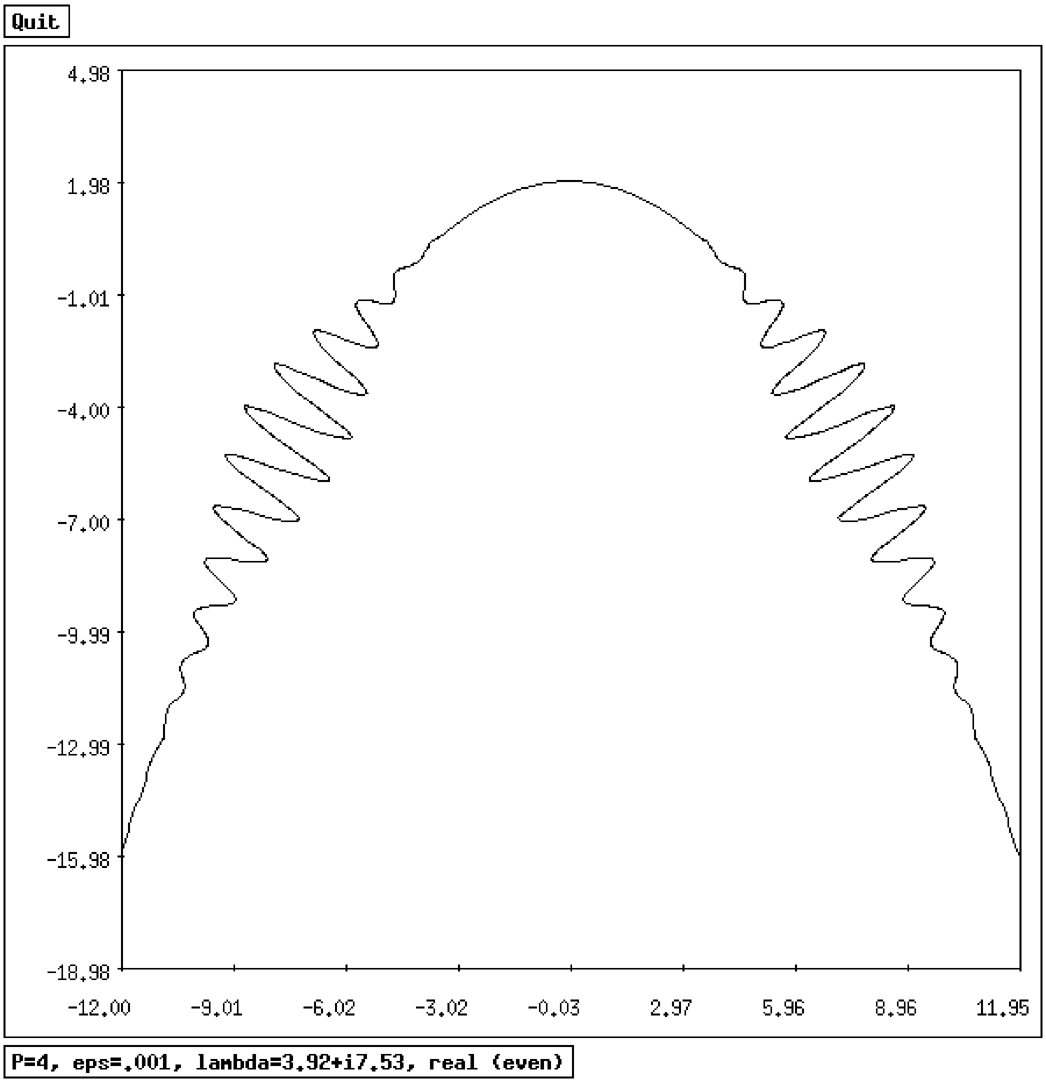

Figure 3: The real part of a localized eigenmode, corresponding to the eigenvalue $\lambda = 3.926 \pm i7.534$ for $\mathcal{P} = 4$, $\epsilon = .001$.

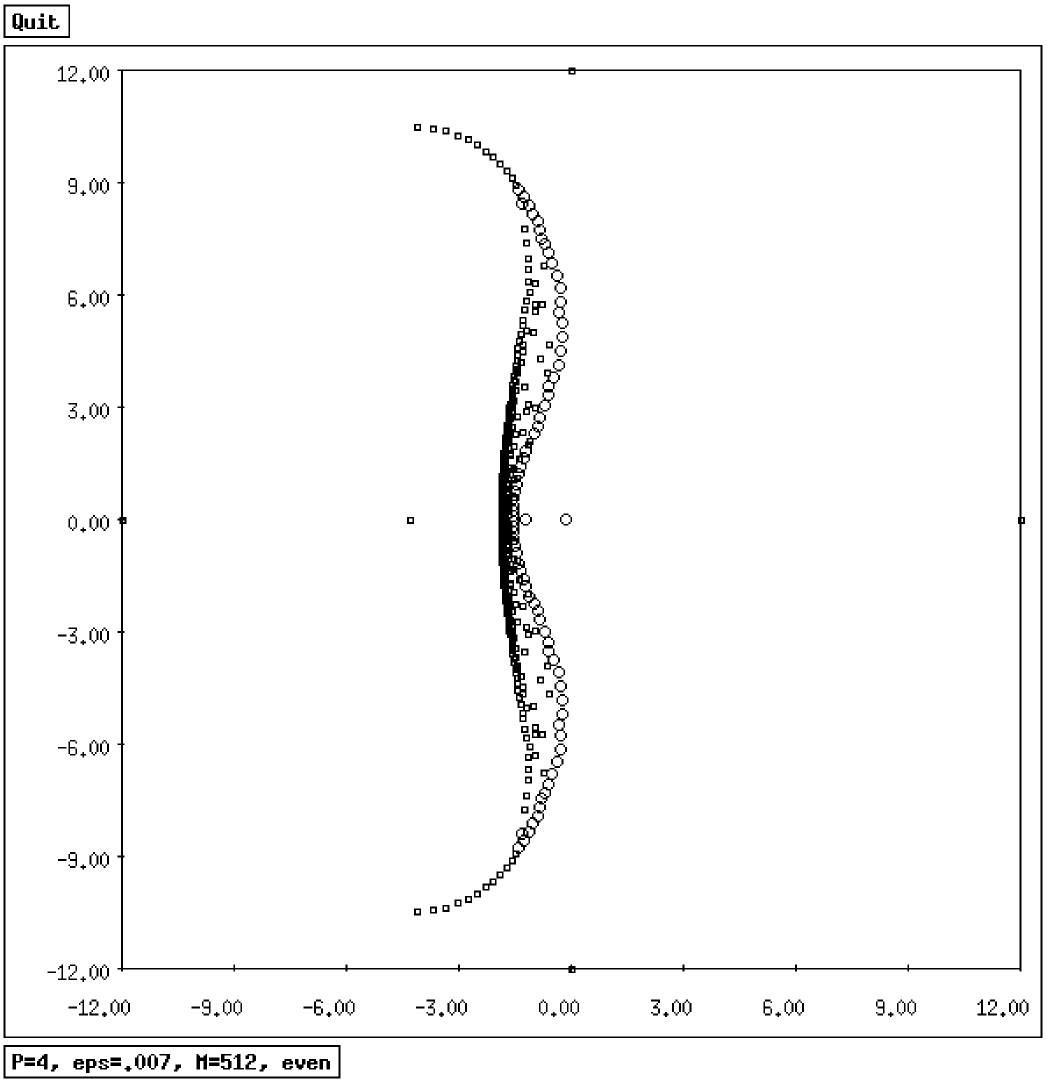

Figure 4: Same as in Fig. 1, with ϵ = .007. All computed eigenvalues have negative real parts.

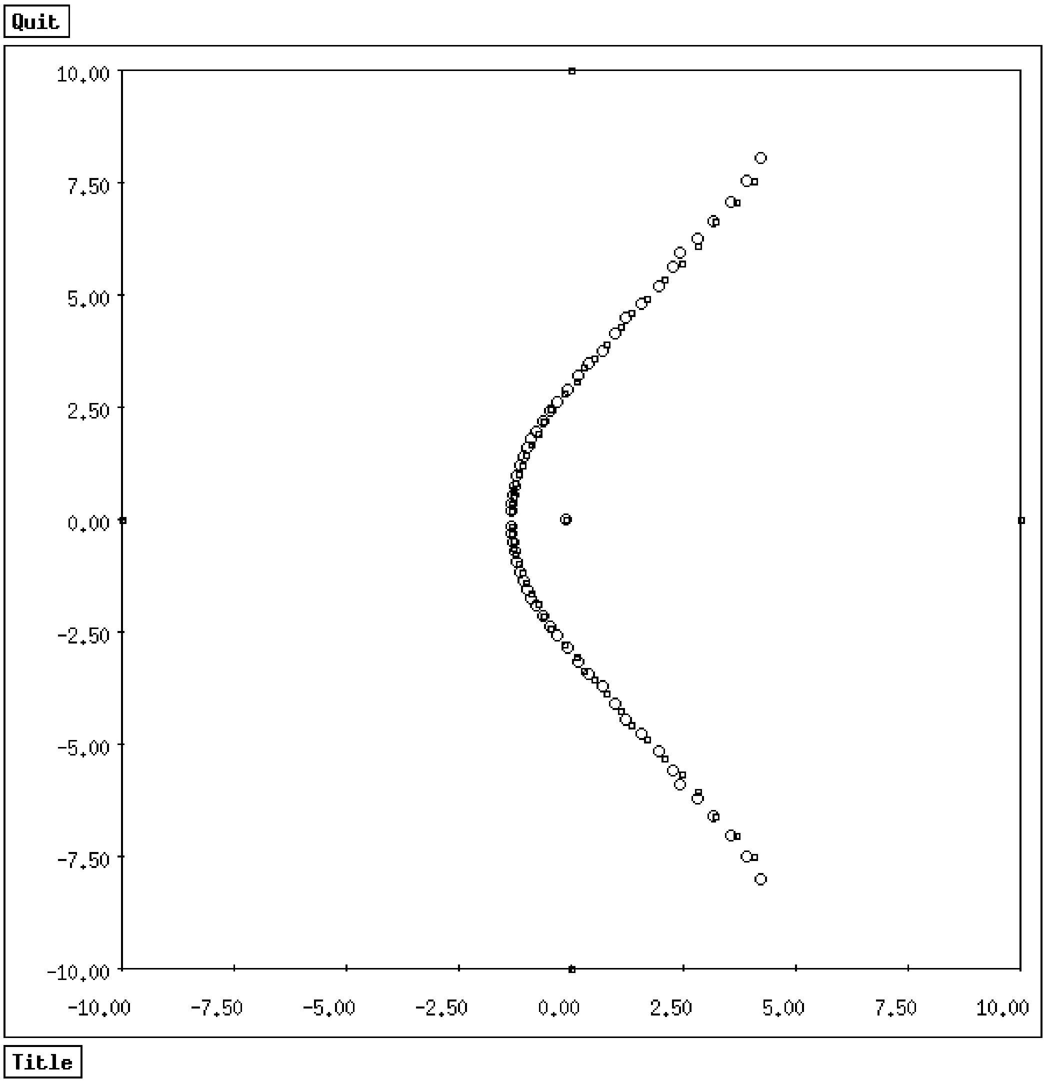

Figure 5: The spectrum for $\mathcal{P} = 4$, with $\epsilon = .001$. Only the proper eigenvalues are shown for truncations $M = 444$ (squares) and $M = 512$ (circles).